Journal of Magnetism and Magnetic Materials 324 (2012) 3129–3132

Contents lists available at SciVerse ScienceDirect

Journal of Magnetism and Magnetic Materials

journal homepage: www.elsevier.com/locate/jmmm

Domain wall nucleation in epitaxial exchange-biased Fe/IrMn bilayers with highly misaligned anisotropies

Wei Zhang, Kannan M. Krishnan *

Department of Materials Science and Engineering, University of Washington, Seattle, WA 98195, USA

ARTICLE INFO

Article history:
Received 14 February 2012
Available online 23 May 2012

Keywords:
Epitaxial thin film
Magnetization reversal
Domain wall nucleation
Exchange bias

ABSTRACT

The angular dependence of the magnetization reversal in epitaxial Fe/IrMn bilayers with collinear and non-collinear cubic and unidirectional anisotropies is investigated. Multistep loops with different magnetization reversal processes are observed for either positive or negative angles with respect to the Fe easy axis. The angular dependence of the switching fields displays the broken symmetry of the induced non-collinearity. The experimental results are reproduced with a generalized domain wall nucleation model that includes the induced anisotropy configuration and the peculiar asymmetric magnetic switching behavior. These results highlight the importance of the relative angle between anisotropies in epitaxial exchange bias systems with incoherent rotation reversal mechanism, opening a new pathway for tailoring the magnetic properties of such systems.

1. Introduction

Ferromagnetic (F)/antiferromagnetic (AF) exchange bias (EB) structures [1] are at the heart of today's spintronics devices, taking advantage of the interfacial exchange interaction effects [2]. Prospects for control and design of desirable magnetic behavior for EB systems depend upon a clear understanding of the key parameters governing the exchange coupling at the interface. Different intrinsic parameters (e.g., materials, anisotropies, thicknesses, and shapes) [2], as well as extrinsic ones (e.g., field cooling (FC) procedures) [3,4] have been explored and characterized [5,6] to understand exchange-coupling phenomena in EB systems. In general, the interfacial exchange coupling effects depend on the nature of the spin-moments at the interface [7] and the strength of competing anisotropies [8], as well as their relative orientation [9,10], that together lead to a complex phase diagram of different reversal behaviors [8–11]. Moreover, the relative importance of the anisotropies involved can be selectively enhanced either intrinsically by interfacial frustration [9,12] or extrinsically via patterning [13–15] and/or special FC procedures [3,4,10,16].

Manipulation of AF interfacial spins with respect to the induced unidirectional anisotropy has been successfully demonstrated in polycrystalline EB systems [9,10] and interpreted by a coherent rotation model. Despite extensive research, there are still ongoing controversies about the fundamental magnetization reversal mechanisms in EB systems. Recent experimental works on epitaxial (002) exchange biased bilayers show inconsistency with the coherent rotation protocol [17–20]. In epitaxial (002) F/AF systems, the interfacial exchange coupling breaks the strong cubic magnetocrystalline anisotropy, resulting in unique multistep hysteresis loops, which can be further interpreted by magnetization reversal via domain wall (DW) nucleation and propagation [20]. The multistep loops make the epitaxial (002) F/AF system a rich paradigm to explore the competing effects between cubic anisotropy and EB. However, previous works only dealt with collinear cubic and exchange anisotropies, where the unidirectional EB easy axis sits along one of the Fe cubic easy axis. In this letter, we describe the magnetization reversal of epitaxial Fe/IrMn bilayers with both collinear and non-collinear anisotropy configurations, and proposed a generalized DW nucleation model to interpret the angular dependent magnetic switching fields. Our work has important practical applications for it reveals the importance of the misalignment between cubic anisotropy and the direction of the applied field during the FC procedure in order to properly account for the asymmetry of the magnetization reversal and the angular dependences of the switching fields.

2. Experimental

Epitaxial $Fe_{15\ nm}/IrMn_{10\ nm}$ bilayers, with a $Ta_{5\ nm}$ capping layer, were grown on transparent MgO(001) substrates (preannealed at 500 °C) by ultrahigh vacuum ion-beam sputtering at an elevated temperature of 145 °C. As shown earlier [20], x-ray $\theta-2\theta$ scans and in-plane Φ-scans have confirmed the epitaxial

* Corresponding author. Tel.: +1 206 543 2814; fax: +1 206 543 3100.
E-mail addresses: zwei@uw.edu (W. Zhang), kannanmk@uw.edu (K.M. Krishnan).

0304-8853/$ - see front matter © 2012 Elsevier B.V. All rights reserved.
http://dx.doi.org/10.1016/j.jmmm.2012.05.016

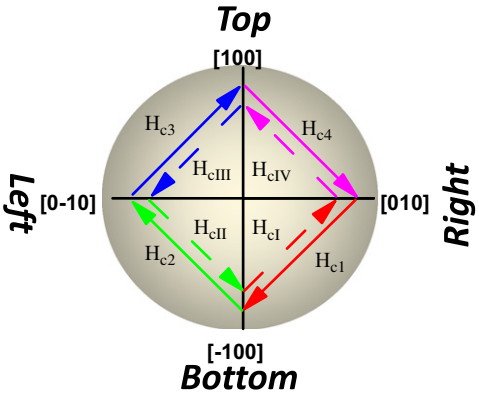

Fig. 1. Definition of the various switching fields between different Fe easy axes. Each 180° magnetization reversal (two-step) involves one of the four semicircles (top, bottom, left, right).

relationship of the Fe/IrMn bilayers, i.e., MgO(001)[100]||-Fe(001)[110]||IrMn(001)[100]. A permanent magnet generating a field of ~300 Oe was employed throughout the sample deposition and cooling process [to room temperature, RT], to define the EB direction. The field direction of the magnet was misaligned by an angle α_{FC} with respect to the Fe[010] easy axis. Two different anisotropy configurations were set by using $\alpha_{FC}=0^\circ$ (collinear) and $\alpha_{FC}=-21^\circ$ (non-collinear). Angular dependent vector magneto-optic Kerr effect (MOKE) [21,22] measurements were performed *ex situ* at RT to study the reversal of both in-plane magnetization components, i.e., longitudinal (||) and transverse (⊥) components at different ϕ ,defined as the angle between the external applied field, H_{ext}, and the Fe[010] easy axis. Previous works have shown that the magnetization reversals are achieved via DW nucleation and propagation along the different Fe easy axes [20,23]. Depending on the initial and final remanent directions involved in a magnetic transition, we refer to the corresponding switching fields as H_{c1}–H_{c4} (clockwise), and H_{cI}–H_{cIV} (counter-clockwise), respectively (Fig. 1).

3. Results and discussions

Fig. 2 compares the in-plane magnetization hysteresis loops at Fe[010] ($\phi=0^\circ$) and Fe[−100] ($\phi=-90^\circ$) for the collinear ($\alpha_{FC}=0^\circ$) and non-collinear ($\alpha_{FC}=-21^\circ$) coupling configurations, respectively. For $\phi=0^\circ$, biased loops with one-step magnetization reversal, for both descending and ascending branches of the hysteresis loop, were observed for the collinear configuration [Fig. 2(a)]. In contrast, for the non-collinear case, biased loops but with two-step magnetic switching were observed for both branches, due to the broken cubic symmetry by the EB [Fig. 2(b)]. The intermediate state indicates the magnetization reversal along Fe[−100]. For $\phi=-90^\circ$, double-shifted loops with two-step switching were observed for both configurations, Fig. 2(c) and (d). However, the intermediate states for both branches are mediated via the same Fe[010] easy axis. Besides, the hysteresis loop also exhibits a shift along the field axis for the non-collinear anisotropy configuration, marked with a vertical dashed line in Fig. 2(d).

An asymmetric magnetization reversal behavior is found for the non-collinear coupled bilayer. The left and right panels of Fig. 3 show the hysteresis loops acquired close to Fe[010] at corresponding negative and positive ϕ values, respectively. For positive ϕ ($0^\circ \le \phi < 45^\circ$), the magnetization reversal for descending and ascending branches always occurred in two steps and in the same bottom semicircle (Fig. 1) as revealed by the transverse

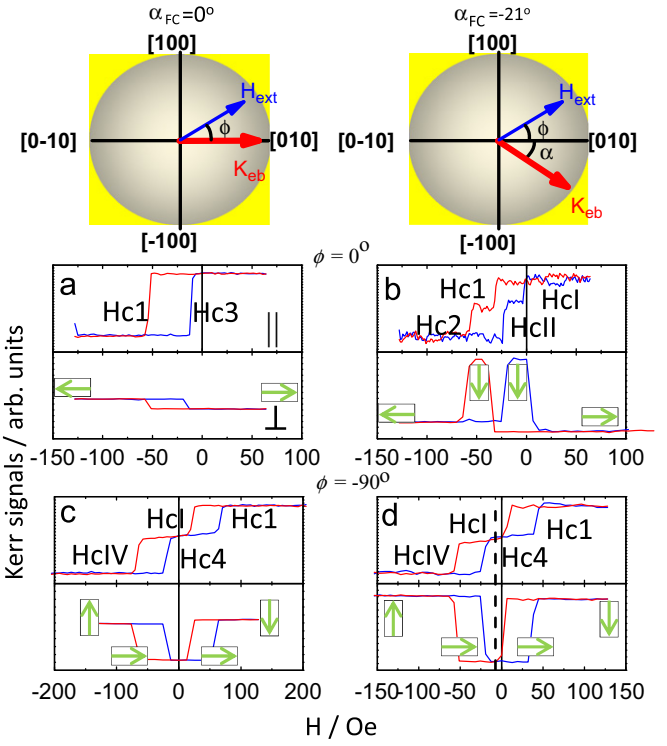

Fig. 2. Longitudinal (||) and transverse (⊥) MOKE loops measured (a,b) at $\phi=0^\circ$ and (c,d) at $\phi=-90^\circ$, with different anisotropy configurations, schematically shown on top, including collinear ($\alpha_{FC}=0^\circ$) and non-collinear ($\alpha_{FC}=-21^\circ$) cases. The orientation of Fe spins in the switching processes is represented by the arrows enclosed in a box.

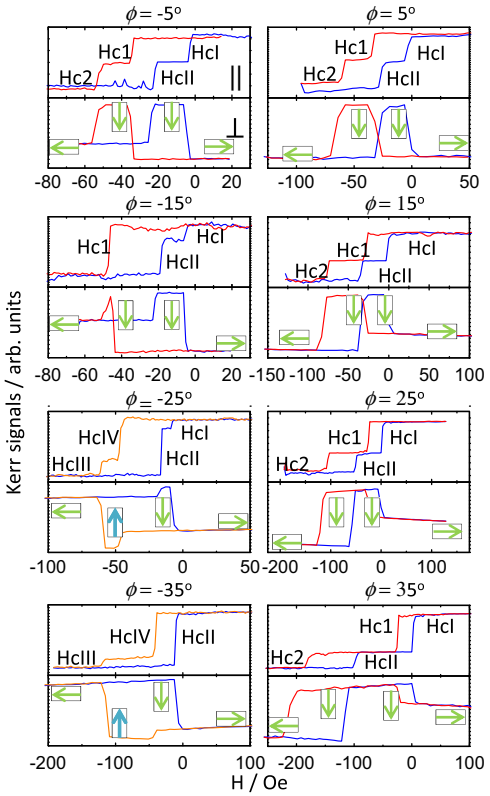

Fig. 3. Longitudinal (||) and transverse (⊥) MOKE loops measured at selective field angles for the non-collinear anisotropy configuration ($\alpha_{FC}=-21^\circ$). The orientation of Fe spins in the switching processes is represented by the arrows enclosed in a box.

MOKE signals, with the intermediate states mediated by Fe[−100]. The magnetic switching occurs via H_{c1} and H_{c2} for the descending branch and the reverse processes, via H_{cII} and H_{cI}, for the ascending branch. For $-15^\circ \le \phi < 0^\circ$, H_{ext} lies between the Fe[010] and the EB directions. Due to the strong K_{eb}, the magnetization reversal still occurs in the bottom semicircle, similar to that for positive ϕ. This is different from the collinear configuration [20], where the magnetization reversal is accommodated by the top semicircle right after H_{ext} passes Fe[010]. For $-45^\circ < \phi \le -25^\circ$ (H_{ext} applied past the EB), the magnetization reversal was accommodated by the top semicircle for descending branch (H_{cIV} and H_{cIII}); however, it still occurs in the bottom semicircle for the ascending branch (H_{cII} and H_{cI}). In other words, the magnetization reversal involves two opposite semicircles (top and bottom), and the intermediate states are mediated by Fe[100] and Fe[−100] for the descending and ascending branches, respectively. This is also significantly different from that of collinear configuration [20], where magnetization reversal involves only the top semicircle for all negative ϕ. It should be noted that for the ascending branch, the second switching at H_{cI} is not observed when $H_{cI} < H_{cII}$, for example at $\phi = -35^\circ$ (Fig. 3). In summary, the magnetization reversal of the non-collinear coupled sample for the corresponding positive and negative values of ϕ shows significant asymmetry as compared with the collinear sample. For the latter [20], the magnetization reversal is symmetric about $\phi = 0^\circ$ and involves only one semicircle for each ϕ.

Next, we propose a generalized DW nucleation model to interpret the ϕ-dependence of the switching fields. Zhan et al. have previously shown that both the one-step and the two-step loops observed in epitaxial Fe/MgO(0 0 1) films are mediated by two successive or two separate 90° DW nucleations [24]. The DW nucleation energy, ε_{90°, can be evaluated by fitting the ϕ-dependence of switching fields. For our Fe/IrMn bilayer system, the AF layer induces an additional anisotropy, K_{eb}. As a result, the total energy for the Fe/IrMn bilayer, with collinear cubic and exchange anisotropies, can be rewritten as

$$E = (K_1/4)\sin^2 2\theta - K_{eb}\cos\theta - MH\cos(\phi-\theta),$$

where θ is the angle between the magnetization M and the Fe[0 1 0] direction. Subsequently, the energies of single domain states at the four Fe easy axes can be obtained as

$$E_{[010]} = -K_{eb} - MH\cos\phi,$$
$$E_{[100]} = -MH\sin\phi,$$
$$E_{[0-10]} = K_{eb} + MH\cos\phi,$$
$$E_{[-100]} = MH\sin\phi.$$

The switching fields related to the DW nucleation energy can be derived from the energy gain between the local minima at the initial and final easy axes involved in the transition [25]. The theoretical switching fields for 90° magnetic transitions, as indicated in Fig. 1, are obtained as

$$H_{c1} = -\frac{\varepsilon_{90^\circ} + K_{eb}}{M(\cos\phi + \sin\phi)},\ H_{c2} = -\frac{\varepsilon_{90^\circ} + K_{eb}}{M(\cos\phi - \sin\phi)},$$

$$H_{c3} = \frac{\varepsilon_{90^\circ} - K_{eb}}{M(\cos\phi + \sin\phi)},\ H_{c4} = \frac{\varepsilon_{90^\circ} - K_{eb}}{M(\cos\phi - \sin\phi)},$$

$$H_{cI} = \frac{\varepsilon_{90^\circ} - K_{eb}}{M(\cos\phi + \sin\phi)},\ H_{cII} = \frac{\varepsilon_{90^\circ} - K_{eb}}{M(\cos\phi - \sin\phi)},$$

$$H_{cIII} = -\frac{\varepsilon_{90^\circ} + K_{eb}}{M(\cos\phi + \sin\phi)},\ H_{cIV} = -\frac{\varepsilon_{90^\circ} + K_{eb}}{M(\cos\phi - \sin\phi)}$$

In our previous work [20], we have shown that this model is in good agreement with the experimental data [26]. Originally, we also included in our model a small induced uniaxial anisotropy, K_u, collinear with K_{eb}. However, fitting for the ϕ-dependence indicated that this induced K_u is negligibly small [20]. Therefore, we no longer consider this term in our generalized DW nucleation model. Detailed discussions on the collinear coupled sample have been reported in the previous work. Just for a brief summary, close to the EB direction, the bottom and top semicircles are involved in the magnetization reversal for $0^\circ < \phi < 45^\circ$ and $-45^\circ < \phi < 0^\circ$, respectively. However, perpendicular to the EB direction, only the right semicircle is involved in the magnetization reversal, with the corresponding switching fields H_{c1}, H_{c4}, H_{cI}, and H_{cIV}. The effective exchange field, K_{eb}/M, as well as ε_{90°/M, of the collinear sample are determined from the fitting as ~33 Oe and ~18 Oe, respectively.

For the non-collinear case as we reported in this work, K_{eb} is decomposed into two components, $K_{eb(||)} = K_{eb}\cos\alpha_{FC}$, and $K_{eb(\perp)} = K_{eb}\sin\alpha_{FC}$, lying along the two orthogonal cubic easy axes. The two orthogonal K_{eb} components act as effective fields superimposed onto the cubic Fe easy axes. Similarly, the theoretical switching fields for 90° magnetic transitions are obtained as

$$H_{c1} = -\frac{\varepsilon_{90^\circ} + K_{eb}(\cos\alpha_{FC} + \sin\alpha_{FC})}{M(\cos\phi + \sin\phi)},$$

$$H_{c2} = -\frac{\varepsilon_{90^\circ} + K_{eb}(\cos\alpha_{FC} - \sin\alpha_{FC})}{M(\cos\phi - \sin\phi)},$$

$$H_{c3} = \frac{\varepsilon_{90^\circ} - K_{eb}(\cos\alpha_{FC} + \sin\alpha_{FC})}{M(\cos\phi + \sin\phi)},$$

$$H_{c4} = \frac{\varepsilon_{90^\circ} - K_{eb}(\cos\alpha_{FC} - \sin\alpha_{FC})}{M(\cos\phi - \sin\phi)},$$

$$H_{cI} = \frac{\varepsilon_{90^\circ} - K_{eb}(\cos\alpha_{FC} + \sin\alpha_{FC})}{M(\cos\phi + \sin\phi)},$$

$$H_{cII} = \frac{\varepsilon_{90^\circ} - K_{eb}(\cos\alpha_{FC} - \sin\alpha_{FC})}{M(\cos\phi - \sin\phi)},$$

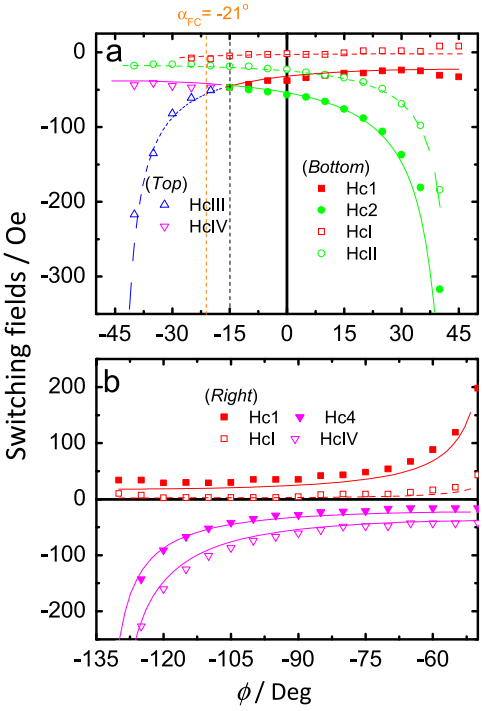

Fig. 4. Angular dependence of the experimentally observed switching fields (symbols) and the corresponding theoretical fitting results (curves) for the non-collinear coupled bilayer. The switching fields, represented by different symbols and curves, correspond to the magnetic transitions between different initial and final Fe easy axes orientations. The semicircles (see Fig. 1) followed by the switching fields during the reversal are also indicated.

$$H_{cIII} = -\frac{\varepsilon_{90^o} + K_{eb}(\cos\alpha_{FC} + \sin\alpha_{FC})}{M(\cos\phi + \sin\phi)},$$

$$H_{cIV} = -\frac{\varepsilon_{90^o} + K_{eb}(\cos\alpha_{FC} - \sin\alpha_{FC})}{M(\cos\phi - \sin\phi)},$$

We applied these equations and fit for the angular dependent switching fields of the non-collinear sample. The ϕ-dependences close to Fe[010] and Fe[-100] are summarized in Fig. 4(a) and (b), respectively. All the switching fields can be nicely fitted with the fitting parameters $K_{eb}/M = 31$ Oe, $\varepsilon_{90^\circ}/M = 14.5$ Oe, and $\alpha_{FC} = -21^\circ$. Because K_{eb}/M and ε_{90°/M are both AF dependent, the slight difference of the fitted values for the two configurations is possibly caused by the AF misalignment. In Fig. 4(a), the symmetry about $\phi = 0^\circ$ is broken. For the descending branch, the magnetization reversal via the top semicircle (H_{cIII} and H_{cIV}) was suppressed by the non-collinear EB. The magnetization reversal via the bottom semicircle (H_{c1} and H_{c2}) became largely favorable. The transition of the magnetization reversal from the bottom to the top semicircle occurred at $\phi \sim -15^\circ$, not at $\alpha_{FC} = -21^\circ$ as one would intuitively expect [Fig. 4(a)]. This is also consistent with our modeling using the above fitting parameters. Physically, the transition angle is dependent on α_{FC} as well as the relative strength of K_{eb} and ε_{90°. For the ascending branch, the magnetization reversal via the top semicircle (H_{c3} and H_{c4}) is completely prohibited; only the reversal via the bottom semicircle (H_{cI} and H_{cII}) is possible. The strong preference of the magnetization reversal along the bottom semicircle is attributed to the enhanced Fe[-100] easy axis by the $K_{eb(\perp)}$ component. In Fig. 4(b), the four characterizing switching fields, H_{c1}, H_{c4}, H_{cI}, H_{cIV}, are all shifted downwards due to the $K_{eb(\perp)}$. As can be seen, our generalized DW nucleation model reproduces the switching fields very well over the entire angular range, by simply taking into account the misalignment angle, $\alpha_{FC} = -21^\circ$.

4. Conclusion

In summary, detailed angle-dependent magnetic studies in epitaxial (002) exchange biased systems with collinear and non-collinear anisotropy configurations are reported, which showed that a number of asymmetries can be induced by the non-collinearity. We developed a generalized DW nucleation model to quantitatively interpret our data. Our work reveals the importance not only of the relative intensity of the different anisotropies in the system but also of the angle between them. Such induced anisotropic behavior can also be used to tailor the magnetic properties in exchange biased systems.

Acknowledgment

This work was supported by NSF-DMR 1063489.

References

[1] W.H. Meiklejohn, C.P. Bean, Physical Review 102 (1956) 1413.
[2] See reviews J. Nogués, I.K. Schuller, Journal of Magnetism and Magnetic Materials 192 (1999) 203;
A.E. Berkowitz, K. Takano, Journal of Magnetism and Magnetic Materials 200 (1999) 552;
R.L. Stamps, Journal of physics D 33 (2000) R247;
M. Kiwi, Journal of Magnetism and Magnetic Materials 234 (2001) 584.
[3] J. Nogues, D. Lederman, T.J. Moran, I.K. Schuller, Physical Review Letters 76 (1996) 4624.
[4] J. Olamit, Z.P. Li, I.K. Schuller, K. Liu, Physical Review B 73 (2006) 024413.
[5] G. Srajer, L.H. Lewis, S.D. Bader, A.J. Epstein, C.S. Fadley, E.E. Fullerton, A. Hoffmann, J.B. Kortright, K.M. Krishnan, S.A. Majetich, T.S. Rahman, C.A. Ross, M.B. Salamon, I.K. Schuller, T.C. Schulthess, J.Z. Sun, Journal of Magnetism and Magnetic Materials 307 (2006) 1.
[6] P. Blomqvist, K.M. Krishnan, H. Ohldag, Physical Review Letters 94 (2005) 107203.
[7] S. Bruck, G. Schutz, E. Goering, X. Ji, K.M. Krishnan, Physical Review Letters 101 (2008) 126402.
[8] J. Camarero, J. Sort, A. Hoffmann, J.M. García-Martín, B. Dieny, R. Miranda, J. Nogués, Physical Review Letters 95 (2005) 057204.
[9] E. Jiménez, J. Camarero, J. Sort, J. Nogués, A. Hoffmann, N. Mikuszeit, J.M. García-Martín, B. Dieny, R. Miranda, Physical Review B 80 (2009) 014415.
[10] E. Jiménez, J. Camarero, J. Sort, J. Nogués, A. Hoffmann, F.J. Teran, P. Perna, J.M. García-Martín, B. Dieny, R. Miranda, Applied Physics Letters 95 (2009) 122508.
[11] F. Radu, A. Westphalen, K. Theis-Bröhl, H. Zabel, Journal of Physics: Condensed Matter 18 (2006) L29.
[12] J. McCord, C. Hamann, R. Schäfer, L. Schultz, R. Mattheis, Physical Review B 78 (2008) 094419.
[13] A. Hoffmann, M. Grimsditch, J.E. Pearson, J. Nogues, W.A.A. Macedo, I.K. Schuller, Physical Review B 67 (2003) 220406.
[14] S.H. Chung, A. Hoffmann, M. Grimsditch, Physical Review B 71 (2005) 214430.
[15] W. Zhang, D.N. Weiss, K.M. Krishnan, Journal of Applied Physics 107 (2010) 09D724.
[16] S. Bruck, J. Sort, V. Baltz, S. Surinach, J.S. Munoz, B. Diney, M.D. Baro, J. Nogues, Advanced Materials 17 (2005) 2978.
[17] K.M. Krishnan, A.B. Pakhomov, Y. Bao, P. Blomqvist, Y. Chun, M. Gonzales, K. Griffin, X. Ji, B.K. Roberts, Journal of Materials Science 41 (2006) 793.
[18] E. Arenholz, K. Liu, Applied Physics Letters 87 (2005) 132501.
[19] Q.F. Zhan, K.M. Krishnan, Journal of Applied Physics 107 (2010) 09D703.
[20] W. Zhang, M.E. Bowden, K.M. Krishnan, Applied Physics Letters 98 (2011) 092503.
[21] J.M. Florczak, E.D. Dahlberg, Journal of Applied Physics 67 (1990) 7520.
[22] H. Ohldag, N.B. Weber, F.U. Hillebrecht, E. Kisker, Journal of Applied Physics 91 (2002) 2228.
[23] S.G. Wang, A. Kohn, C. Wang, A.K. Petford-Long, S. Lee, R. Fan, J.P. Goff, L.J. Singh, Z.H. Barber, R.C.C. Ward, Journal of Physics D: Applied Physics 42 (2009) 225001.
[24] Q.F. Zhan, S. Vandezande, K. Temst, C. Van Haesendonck, Physical Review B 80 (2009) 094416.
[25] R.P. Cowburn, S.J. Gray, J.A.C. Bland, Physical Review Letters 79 (1997) 4018.
[26] The effective fields, H_X and H_A as they appear in Ref. [20], equal K_{eb}/M and ε_{90°/M, respectively, here.